Understanding the isomerization kinetics in the gas phase of a triazole-3-thione derivative: A theoretical approach

ZAHRA KAZEMINEJAD[1], ABOLFAZL SHIROUDI[2]*, KHALIL POURSHAMSIAN[1]**,
FARHAD HATAMJAFARI[1] and AHMAD REZA OLIAEY[1]

[1]*Department of Chemistry, Tonekabon Branch, Islamic Azad University, Tonekabon, Iran and*
[2]*Young Researchers and Elite Club, East Tehran Branch, Islamic Azad University,
Tehran, Iran*

Abstract: The isomerization reactions of the 4-amino-5-methyl-2,4-dihydro--3*H*-1,2,4-triazole-3-thione were studied using the B3LYP and M06-2*x*, as well as the CBS-QB3 theoretical methods. The measured energy profiles were complemented with kinetic rate constants using the transition state theory (TST). Based on the isomers geometries optimized using the CBS-QB3 method, a natural bond orbital (NBO) analysis shows that the stabilization energies of non-bonding lone-pair orbitals [LP(e)$_{S7}$] to the σ*$_{N2-C3}$ antibonding orbital increase from isomers **1** to **2**. Moreover, the LP(e)$_{S7}$ → σ*$_{N2-C3}$ delocalizations could fairly explain the increase in the occupancies of LP(e)$_{S7}$ orbitals for isomers **1** and **2** (**2** > **1**). The studied stabilization energy increases the stability of the ground state structure, and could fairly explain the kinetics of the isomerization reactions 1 and 2 ($k_2 > k_1$). NBO results also suggest that the kinetics of these processes are controlled by the LP → σ* resonance energies.

Keywords: isomerization; rate constant; chemical kinetics; DFT; NBO.

INTRODUCTION

Triazoles are known as isosteres of imidazoles that are prominent medicinal moieties in which the carbon atoms are isosterically replaced by nitrogen.[1] The chemistry involving triazoles has a vital role due to their industrial and medicinal characteristics in the pharmaceutical industry.[2,3] Furthermore, 1,2,4-triazole derivatives were revealed to possess a broad-spectrum of biological activities,[4–7] and the disubstituted 1,2,4-triazole derivatives have a much greater biological activity than the parent molecule.[8,9] 1,2,4-Triazole derivatives are important compounds in medicinal chemistry.[10] Moreover, the presence of a sulfur atom at the 3-posit-

---

*,** Corresponding authors. E-mail: (*)abolfazl.shiroudi@iauet.ac.ir;
(**)kshams49@gmail.com

975

ion of 1,2,4-triazole is essential to enhance various types of biological activities.[11,12] The 1,2,4-triazoles have been incorporated into a wide variety of therapeutically important agents such as ribavirin with antiviral, rizatriptan as antimigraine, letrozole and anastrozole showing antitumor activity which is currently being used for the treatment of breast cancer due to the biological activities.[13–17]

Having two vital and stable factors in metabolic non-degradation related to drug targets[18] and forming hydrogen bonds, triazoles are biologically considered active molecules as pharmacophores.[19,20] The recorded pharmacological activities are antibacterial,[21] antifungal,[22] antiviral,[23] anticonvulsant,[24,25] anti-inflammatory,[26] anticancer[27,28] and antidepressant, while as 1,2,4-triazoles have an effect on the central nervous system, they could be great drugs as stimulants and anxiolytics.[27] Thiadiazoles and triazoles are well-known for their valuable anti-tuberculosis, antibacterial, and anticonvulsant properties.[29]

The knowledge and understanding of the relative stabilities of tautomeric forms and any subsequent conversions between the tautomeric forms are also important from structural chemistry viewpoints.[12] Furthermore, knowing how the tautomerization energies change in various derivatives gives insight into the influence of substituents on molecular stability and reactivity. Thus, it is worth studying the possibility of tautomerization in the parent molecule of 1,2,4-triazole-3-thione and its derivatives using high accuracy methods.[30]

In recent years, some theoretical and experimental studies have highlighted the importance of stabilities of tautomeric forms of the 1,2,4-triazoles and their derivatives as well as the subsequent conversions between tautomeric forms. The described transformation should formally be treated as 1,3-sigmatropic proton shift in the heteroallylic system.
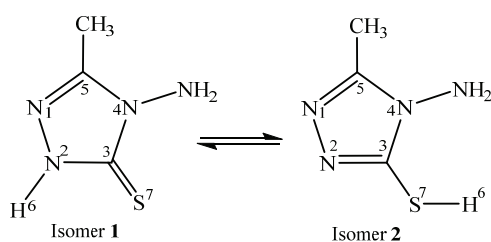
Fotouhi *et al.*[31] experimentally studied the electro-oxidation of 4-amino-5-methyl-2,4-dyhydro-3*H*-1,2,4-triazol-3-thione in acetate buffer (pH 4.6, 10 vol.% methanol) at a glass carbon electrode (GCE), which was investigated using direct current (DC), differential pulse voltammetry (DPV), cyclic voltammetry (CV), choronoamperemetry, rotating disk electrode (RDE) and coulometry in order to investigate the electrochemical behavior of some metal complexes of mercaptotriazoles to be synthesized in the future.

In a recent study, Gökce *et al.*[32] performed an investigation of the molecular structure (thione–thiol tautomerism) at the B3LYP/6-311++G(d,p) theoretical level in the gas phase as well as experimental records that were obtained for all tautomeric forms of the 5-(3-pyridyl)-4*H*-1,2,4-triazole-3-thiol molecule in solid phase of isolated molecule.

Davari *et al.*[12] theoretically studied the optimized parent molecule of 1,2,4-triazole-3-thione and its thiol form using HF, B3LYP, and MP2 methods employing various basis sets, including various Pople and Dunning basis sets. However, in the

present work, we wish to supply detailed computations of the kinetic rate constants for the isomerization reactions of 4-amino-5-methyl-2,4-dihydro-3*H*-1,2,4-triazole-3--thione and its thiol form at a pressure of 1 bar and $T = 298$ K. For this purpose, use was made of the transition state theory (TST) employing the density functional theory (DFT)[33] together with a variety of exchange-correlation functionals, namely, the Becke-3-parameters–Lee–Yang–Parr (B3LYP) functional,[34,35] and the M06-2*x* functional,[36,37] in conjunction with aug-cc-PVTZ basis set.[38] In some cases, the basis set is about twice as large as some Pople basis sets that were employed by Davari *et al.*[12]

The reaction energies and energy barriers, as well as thermodynamic parameters, were calculated at the B3LYP and M06-2*x* theoretical levels, and then a comparison was made with the composite CBS-QB3 method[39] in order to gain further quantitative theoretical insights into the studied tautomeric reactions, shown in Scheme 1, to determine which exchange-correlation functional gives the most accurate energy barriers and reaction energies. It was found that the DFT methods alone are insufficient for quantitatively investigating the potential energy surface of the reaction mechanisms and kinetics processes given the inability of many popular DFT functionals to describe quantitatively non-bonded interactions and barrier heights. The DFT (B3LYP and M06-2*x*) functionals in conjunction with aug-cc-pVTZ basis set[38] will be used, and then the calculated energy barriers and reaction energies will be compared with the CBS-QB3 results. Furthermore, rate constants will be calculated in the high-pressure limit using TST[40] under atmospheric condition. Finally, an attempt will be made to supply further qualitative chemical insights into the involved reaction mechanisms by analyzing the results achieved using bond order, donor–acceptor interaction energies and natural bond orbital (NBO) occupancies.[41,42]

Scheme 1. The structures of the isomers of 4-amino-5-methyl-2,4-dihydro-3*H*-1,2,4--triazole-3-thione.

COMPUTATIONAL DETAILS

All calculations of the electronic structure were realized by means of the Gaussian 09 software package.[43] The molecular structures and vibrational frequencies of all stationary points were computed at the B3LYP/aug-cc-pVTZ and M06-2*x*/aug-cc-pVTZ theoretical levels. The rationale behind choosing the M06-2*x* exchange-correlation functional is that a recent study by Zhao and Truhlar showed that it is the best one for applications involving main-group thermochemistry, kinetics, noncovalent interactions, and electronic excitation

energies to valence and Rydberg states. The M06-2*x* exchange-correlation functional and its analogs are dedicated for precise energetic considerations.[37] However, in some cases, this approach could underestimate the values of the activation parameters, which was recently confirmed.[44] Therefore, the application of this functional without verification using B3LYP functional is not recommended.

The nature of all optimized structures was determined according to vibrational frequencies calculations, which were calculated at the same levels. The energies of the stationary points were refined by the CBS-QB3 theoretical method. The energies of all the studied stationary points were re-evaluated using the CBS-QB3 model, which includes low-level calculations on large basis sets, mid-sized sets for second-order correlation corrections, and small basis sets for high-level correlation corrections. The five-step CBS-QB3 series of calculations starts with a geometry optimization at the B3LYP/6-311G(2d,d,p) level, followed by a frequency calculation to obtain thermal corrections, zero-point vibrational energy, and entropic information.[45] In order to calibrate the accuracy of the B3LYP and M06-2*x* functionals, employing the CBS-QB3 composite method seemed to be necessary in this work.

The intrinsic reaction coordinate (IRC) analysis[46] was performed in both directions (forward and backward) along the reaction path in order to check the energy profiles connecting the identified transition state structure to the associated energy minima.[47] TST calculations were performed in conjunction with a detailed exploration of the IRC path at the B3LYP/6-31G** level. Thirty points in both directions from the transition state position, IRCs in mass-weighted Cartesian coordinates were generated in this work for each reaction with a 0.1 amu$^{1/2}$ Bohr step size. IRC calculations demonstrated that the transition state structure connects the reactant (isomer 2) and product (isomer 1). The IRC reaction profile is shown in the Supplementary material to this paper (Fig. S-1).

Kinetic rate constants and thermodynamic parameters of the reactions **1** and **2** were calculated in the high-pressure limit by implementation of TST under atmospheric conditions in the KiSThelP package.[48] Kinetic rate constant using transition state theory, $k_{TST}(T)$, of the tautomeric reactions at $T = 298$ K is calculated using TST as given by:[49,50]

$$k_{TST}(T) = \kappa(T)\frac{\sigma k_B T}{h}\frac{Q_{TS}^{\neq}}{Q_R}\exp\left(-E^{\neq}/k_B T\right) \qquad (1)$$

where k_B and h are the Boltzmann's and Planck's constants, respectively, T is the absolute temperature, σ is the reaction symmetry number, $\kappa(T)$ denotes the Wigner tunneling correction factor,[51,52] and $E^{\neq}$ is the activation energy. In the above equation, $Q^{\neq}$ and Q_R represent the total molecular partition functions per unit volume for the transition state and the reactant, respectively. Reaction symmetry number $\sigma = 1$ is taken into consideration for the studied reactions.

<div align="center">RESULTS AND DISCUSSION</div>

Energetic and thermodynamic parameters

Changes in activation enthalpy ($\Delta H^{\neq}$), activation Gibbs energy ($\Delta G^{\neq}$) and reaction energies (ΔH and ΔG) at 298 K for the reactions (1) (isomer **1** → isomer **2**) and (2) (isomer **2** → isomer **1**) are summarized in Table I. The different levels calculations show that reaction (1) is an endothermic process, ΔH_{298K} ranging from 14 to 15 kcal* mol^{-1}, depending on the employed functional. At $p = 1$ bar

---

* 1 kcal = 4184 J

and $T = 298$ K, $\Delta G°_s$ for reaction (2) is negative, hence it is exergonic process, while this parameter for reaction (1) is positive, *i.e.*, endogenic process. As could be seen from Table I, $\Delta H°^{\neq}$ and $\Delta G°^{\neq}$ of the reaction (1) are positive; thus the activation processes require energy and are not spontaneous. It appears that the production of the isomer **1** species *via* reaction (2) is the more favored reaction, since the studied reaction is strongly exergonic with $\Delta G°_{298K}$ ranging from -15.2 to -13.4 kcal mol^{-1}, and strongly exothermic process with $\Delta H°_{298K}$ ranging from -15 to -14 kcal mol^{-1}.

TABLE I. Reaction and activation parameters for the isomerization reactions at different levels ($p =1$ atm)

Parameter kcal mol^{-1}	Reaction (1) (isomer **1** → isomer **2**)			Reaction (2) (isomer **2** → isomer **1**)		
	B3LYP	M06-2*x*	CBS-QB3	B3LYP	M06-2*x*	CBS-QB3
ΔE_{0K}	14.8	14.5	13.7	−14.8	−14.5	−13.7
$\Delta H°_{298K}$	15.0	14.2	14.0	−15.0	−14.2	−14.0
$\Delta G°_{298K}$	14.6	15.2	13.4	−14.6	−15.2	−13.4
$\Delta E_{0K}^{\neq}$	43.7	44.7	43.4	28.9	30.2	29.7
$\Delta H°_{298K}^{\neq}$	43.6	44.5	43.3	28.6	30.4	29.3
$\Delta G°_{298K}^{\neq}$	43.7	45.2	43.3	29.1	30.0	29.9

DFT calculations (B3LYP and M06-2*x*) as well as CBS-QB3 method demonstrate that the energy barrier ($\Delta E_{0K}^{\neq}$) characterizing the formation of isomer **1** species is generally lower by 13.7–14.5 kcal mol^{-1} than that for reaction (1). Similar observations could be made when $\Delta G^{\neq}$ values are considered in spite of slightly unfavorable entropies; the values for reaction (2) (29.1–30.0 kcal mol^{-1}) are lower than those for reaction (1) (43.3–45.2 kcal mol^{-1}). Such differences for the studied pathways indicate that the formation of isomer **1** species will be kinetically favored over the formation of isomer **2** (see Fig. 1).

The predicted vibrational frequencies and rotational moments of inertia for the stationary points involved in the chemical reactions (1) and (2) at the studied theoretical methods are summarized in the Supplementary material (Tables S-I and S-II). The scaling factors of 0.968, 0.971 and 0.99 were imposed on the calculated frequencies at the B3LYP/aug-cc-PVTZ, M06-2*x*/aug-cc-pVTZ and CBS-QB3 levels of theory, respectively.[53]

Structural characteristics of stationary points

The geometrical characteristics of all stationary points in the studied reactions at all the theoretical levels are supplied in the Table S-III, Supplementary material, and are shown in Fig. 2.

Atom numbers are given in Scheme 1 for clarity. The TS structure for the isomerization of the studied compound *via* reaction (2) is a four-membered cyclic structure. The most significant geometrical change is observed for the

N_2–H_6 bond, which shrinks by 0.36–0.38 Å in the structure of isomer **1** compared with the transition state. The S_7–H_6 bond length similarly increases by 0.37–0.38 Å along reaction (2), indicating a breaking of this chemical bond in the transition state. Inspection of the N_2–C_3 bond lengths revealed changes from double to single bond character, with the bond lengths increasing from 1.301 to 1.319 Å in TS at the CBS-QB3 composite method (see Fig. 2). In line with the given geometrical parameters, the dihedral angles in TS structure for reaction (2) have a geometry with the ring almost planar. At the B3LYP, M06-2*x* and CBS-QB3 levels, the imaginary frequencies for the TS are found to be 1635.5*i*, 1639.6*i* and 1624.6*i* cm^{-1}, respectively.
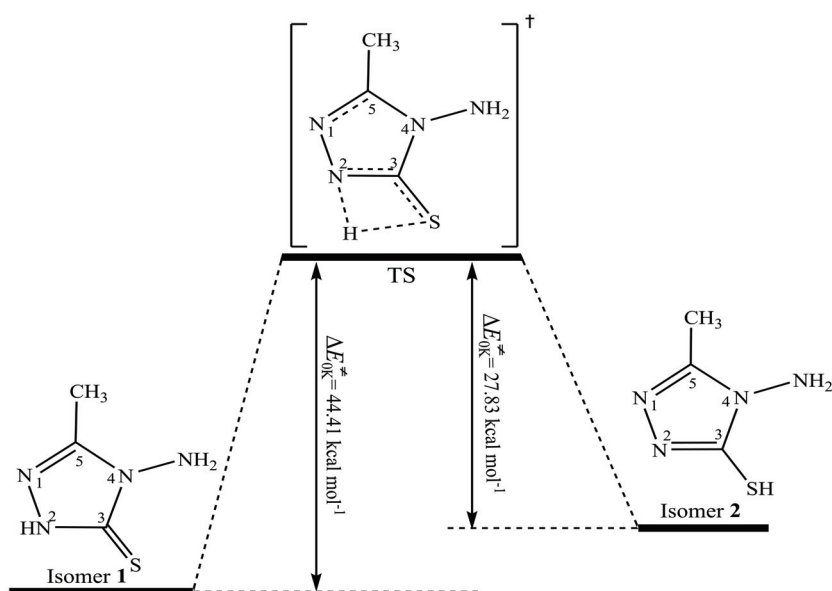

Fig. 1. Energy profile for the isomerization reaction (isomer **1** → isomer **2**) at the CBS-QB3 level.
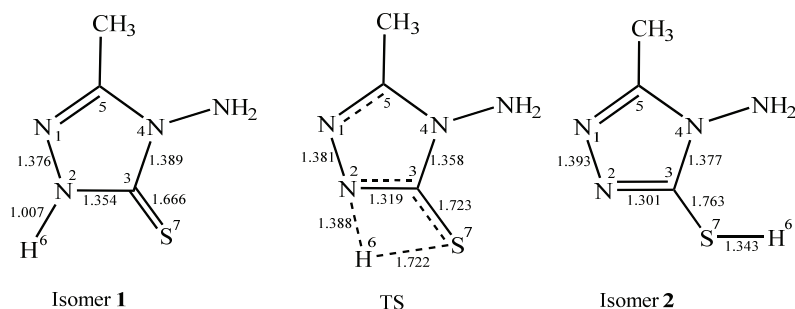

Fig. 2. All stationary points involved in the isomerization reactions (1) and (2) at the CBS-QB3 level.

According to the Hammond postulate, the position of the TS structure along the reaction coordinate is given by the n_T parameter, which is defined as follows:[54,55]

$$n_T = \frac{1}{2 - (\Delta G^o / \Delta G^{\neq})} \tag{2}$$

The n_T values for the reactions (1) and (2) are equal to ≈0.6 and ≈0.4, respectively. The calculated results show that reaction (1) is characterized by a transition state that is closer to isomer **2**.

Kinetic parameters

Kinetic rate constants for the isomerization reactions (1) and (2) at a pressure of 1 bar and $T = 298$ K are given in Table II. Rate constants are the results of TST calculation performed using different quantum chemical data. Under atmospheric conditions, the rate constant for reaction (2) is larger than that obtained for reaction (1), which is in line with the reduction of the activation energy barrier by 13.7–14.8 kcal mol^{-1}. As expected, because of the involved positive energy barrier, the rate constant will increase gradually with increasing temperature. At a pressure of 1 bar, the formation of the isomer **1** species will therefore clearly predominate over the formation of the isomer **2** species. These results indicate that reaction (2) is from both thermodynamic and kinetic viewpoints more favorable than the chemical reaction (1).

TABLE II. The temperature-dependent rate constants for the studied reactions and fitted modified Arrhenius parameters ($k = T^n \exp(-E_a/RT)$) calculated by TST ($p = 1$ bar, $T = 298$ K) at different levels.

Parameter	Method		
	B3LYP/aug-cc-pVTZ	M06-2x/aug-cc-pVTZ	CBS-QB3
Reaction (1) (isomer **1** → isomer **2**)			
k / s^{-1}	1.98×10^{-16}	1.02×10^{-17}	5.45×10^{-16}
A / s^{-1}	6.61×10^{12}	3.89×10^{12}	8.95×10^{12}
$\kappa(T)$	3.60	3.46	3.51
E_a / kcal mol^{-1}	39.14	40.41	38.71
Reaction (2) (isomer **2** → isomer **1**)			
k / s^{-1}	6.36×10^{-8}	2.13×10^{-9}	1.88×10^{-8}
A / s^{-1}	1.04×10^{14}	5.74×10^{13}	1.34×10^{14}
$\kappa(T)$	3.40	3.23	3.28
E_a / kcal mol^{-1}	27.07	28.59	27.85

All the obtained temperature-dependent TST rate constants and fitted modified Arrhenius parameters for the chemical reactions (1) and (2) are presented in Table II. Detailed inspection of Table II shows that the rate constants calculated at $p = 1$ bar by the TST approaches in conjunction with the same energy profiles

are positively dependent on the tunneling effect on the kinetic reaction rate. The Wigner tunneling factor for favorable reaction (2) is shown to have an influence on the kinetic rate constant. Indeed, based on the computed energy profiles and vibrational frequencies, the $\kappa(T)$ values related to the tunneling, ranging from 3.46 to 3.6 found for TST calculations of the kinetic rate constants, characterize the studied pathways.

Bond order analysis

A further balanced measure of bond-breaking/bond-forming along the chemical reaction is delivered using bond order (B) concepts in order to consider the molecular mechanism.[41,56,57] Wiberg bond indices (B_i)[58] are computed based on NBO analysis.[59] There are several breaking/forming bonds occurring during the reactions (1) and (2) that are given by the synchronicity (S_y) index[60] that is defined by:

$$S_y = 1 - \frac{\left[\sum_{i=1}^{n} \dfrac{|\delta B_i - \delta B_{av}|}{\delta B_{av}} \right]}{2n - 2} \tag{3}$$

where n is the number of bonds that are directly involved in the process, δB_i is the relative variation of the bond index for bond i at the TS, δB_{av} is the average bond index variation, and EV represents evolution through the reaction coordinate $(EV / \% = 100\delta B_i)$. The magnitude of the value for the synchronicity parameter varies between 0 and 1.[61] Bond indices were calculated for the chemical bonds that are involved in the isomerization reaction, *i.e.*, the N_2–H_6, N_2–C_3, C_3–S_7 and H_6–S_7 bonds (see Scheme 1 for atom numbering). All other bonds remain practically unaltered. The calculated Wiberg bond indices B_i for the reactant, transition state and product enable the reaction progress to be examined and to evaluate the position of the transition states between reactant and product (Table III).

TABLE III. Bond order analysis of the structures involved in the pathways **1** and **2** at the CBS-QB3 level

Reaction	Parameter	Bond					
		N_2–H_6	N_2–C_3	C_3–S_7	H_6–S_7	δB_{av}	S_y
Reaction (1)	B_i(R)	0.7930	1.2051	1.5063	0.0015	0.5851	0.933
(isomer **1** → isomer **2**)	B_i(TS)	0.3422	1.4157	1.2071	0.4896		
	B_i(P)	0.0063	1.5863	1.0811	0.9533		
	$EV / \%$	57.303	55.089	70.367	51.282		
Reaction (2)	B_i(R)	0.0063	1.5863	1.0811	0.9533	0.4145	0.905
(isomer **2** → isomer **1**)	B_i(TS)	0.3422	1.4157	1.2071	0.4896		
	B_i(P)	0.7930	1.2051	1.5063	0.0015		
	$EV / \%$	42.697	44.753	29.633	48.718		

Reaction (1) leads to cleavage of the N_2–H_6 bond to yield a product located 13.7–14.8 kcal mol^{-1} above the reactant at the studied theoretical levels. The transition state results from a simple elongation of the breaking N_2–H_6 chemical bond and the simultaneous shrinkage of the H_6–S_7 distance because of forming the H_6–S_7 simple bond. The N_2–H_6 bond is elongated by 1.369–1.388 Å, and the H_6–S_7 bond formed is longer than the equilibrium bond length in isomer **2** species. The Wiberg bond indices show that for the isomerization reaction (1), the changes in the C_3–S_7 bond (EV = 70.37 %) progress more than N_2–H_6 bond breaking (EV = 57.30 %), the H_6–S_7 bond forming (EV = 51.28 %), and changes in the N_2–C_3 bond (EV = 55.09 %). Less progress is observed in the H_6–S_7 simple bond formation. The synchronicity index for this reaction is equal to 0.933, which indicates that the studied channel could be described as one-step and slightly asynchronous.

Reaction (2) leads to cleavage of the H_6–S_7 bond through TS to produce isomer **1**, located at 13.7–14.8 kcal mol^{-1} below the reactant (isomer **2**) at all levels of theory. The transition state results from a simple elongation of the breaking H_6–S_7 bond and the simultaneous shrinkage of N_2–H_6 due to the formation of the N_2–H_6 simple bond. The H_6–S_7 bond is elongated to 1.713–1.728 Å, and the forming N_2–H_6 bond is longer than the equilibrium bond length. Moreover, in this reaction, the evolution in the bond breaking of H_6–S_7 (48.72 %) is more progressed than the N_2–H_6 bond forming, and changes in the N_2–C_3 bond (EV = 44.75 %). On the other hand, N_2–C_3 bond changes from a double to a single bond.

Changes in electron distribution during the reaction can be studied by means of charges. NBO charges have been proved to be useful in this sense. The NBO charges for isomers **1** and **2** and also the transition state are reported in Table IV, with atom numbering being the same as that given in Scheme 1. Analysis of NBO charges as the reaction proceeds from reactant to transition state in the reactions (1) and (2) demonstrates that the following changes in partial charges occur:

– In reaction (1), the increase in positive charges δ^+ on carbon C_3 (0.209) in isomer **1** compared to 0.236 in TS with changes in the C_3–S_7 bond, an increase in negative charge δ^- on sulfur S_7 (–0.278) in the isomer **1** compared to –0.171 in TS.

– in reaction (2), the increase in positive charges δ^+ on hydrogen H_6 (0.163) in isomer **2** compared to 0.339 in TS as H_6–S_7 bond breaks and an increase in negative charge δ^- on sulfur S_7 (0.001) in the isomer 2 compared to –0.171 in TS.

Compounds with resonance structures often have chemical bonds that are not easily described as single or double bonds. Thus, in this case, bond order indicates the type and strength of covalent bonds between atoms. Bond order

between N_1 and C_5 of isomer **1** is 1.626 whereas bond order between same atoms (N_1–C_5) of isomer **2** is 1.612 (Fig. 3).

TABLE IV. NBO charges of isomers **1** and **2**, and the transition state for the isomerization reactions at the CBS-QB3 level

Atom	Species		
	Isomer **1**	TS	Isomer **2**
N_1	–0.29929	–0.28281	–0.30919
N_2	–0.37732	–0.41659	–0.33800
C_3	0.20894	0.23550	0.22425
N_4	–0.26303	–0.26245	–0.27314
C_5	0.41712	–0.61639	0.38982
H_6	0.41887	0.33904	0.16253
S_7	–0.27833	–0.17126	0.00145

The bond between N_1 and C_5 of isomer **1** shows more double bond character than the same bond of isomer **2**. In contrast, bond order between N_2 and C_3 of isomer **1** is 1.205 and bond order between the same atoms of isomer **2** is 1.586. Hence, it is obvious that there are two resonance forms for both isomers mentioned in Fig. 3 but contribution of some resonance forms is greater than the others. Furthermore, dominant resonance structure is determined by the electronic structure of the substituent.
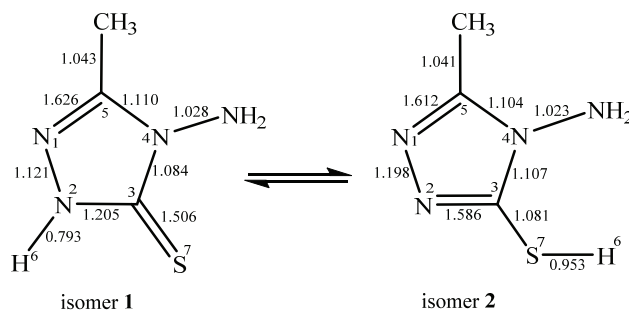

Fig. 3. Bond orders for the dominant resonance forms.

Natural bond orbital analysis

Delocalization of the electron density between occupied (bonding or lone pair [LP]) Lewis type NBO orbitals and empty (antibonding and Rydberg) non--Lewis NBO orbitals imply stabilizing donor–acceptor interactions. The energies of these interactions can be evaluated according to second-order perturbation energies (E_2),[24] which for each donor NBO(i) and acceptor NBO(j) is given by:[62]

$$E_2 = \Delta E_{ij} = q_i \left[\frac{F_{(i,j)}^2}{\varepsilon_i - \varepsilon_j} \right] \qquad (4)$$

where ε_i and ε_j represents the diagonal matrix of the orbital energies, $F_{(i,j)}$ denotes the off-diagonal NBO Fock matrix elements, and q_i is the donor orbital occupancy.

Based on the B3LYP/6-311G(2d,d,p) optimized geometries and electronic structure characteristics of the isomers **1** and **2**, the NBO analysis of donor–acceptor interactions (Table V) revealed that the stabilization energies (E_2) associated with the electronic delocalization from non-bonding sulfur lone-pair [LP(e)$_{S7}$] to σ^*_{N2-C3} antibonding orbitals increases from isomer **1** to isomer **2**. The LP(e)$_{S7} \rightarrow \sigma^*_{N2-C3}$ resonance energies for isomers **1** and **2** are 4.28 and 4.41 kcal mol^{-1}, respectively. The occupancies of the σ_{N2-C3} bonds increase in the following order: isomer **1** < isomer **2**, while the occupancies of σ^*_{N2-C3} bonds increase in a parallel manner in the opposite order (Table V). Furthermore, the NBO results revealed that with increasing LP(e)$_{S7} \rightarrow \sigma^*_{N2-C3}$ resonance energy, energy barrier heights of the isomerization reaction (ΔE_o) around the four-membered rings decrease from isomers **1** to **2**.

TABLE V. NBO occupancies and stabilization energies (E_2) characterizing isomers 1–2 and transition structures along the isomerization reactions based on the CBS-QB3 method

Parameter	Species		
	Isomer **1**	TS	Isomer **2**
Occupancies			
σ_{N2-C3}	1.98849	1.98628	1.98880
σ^*_{N2-C3}	0.07279	0.03245	0.02650
LP(e)S$_7$	1.98710	1.98764	1.98712
Stabilization energy, kcal mol^{-1}			
LP(e)S$_7 \rightarrow \sigma^*_{N2-C3}$	4.28	0.99	4.41

CONCLUSIONS

The isomerization kinetics of 4-amino-5-methyl-2,4-dihydro-3*H*-1,2,4-triazole-3-thione were studied computationally in the gas phase at different DFT (B3LYP and M06-2*x*) and CBS-QB3 methods. The calculated energy profiles were supplemented with calculations of rate constants under atmospheric conditions using the conventional transition state theory. The supplied data indicated that reaction (2) (isomer **2** $\rightarrow$ isomer **1**) is from both thermodynamic and kinetic viewpoints more favorable than the reaction (1) (isomer **1** $\rightarrow$ isomer **2**). The transition states of these reactions correspond to planar four-membered cyclic structures. Analysis of these pathways using synchronicity indices indicated one-step and slightly asynchronous processes. NBO analysis revealed that the stabilization

energy associated with the electronic delocalization from the non-bonding lone-pair (LP(e)$_{S7}$) to σ^*_{N2-C3} antibonding orbitals (LP(e)$_{S7} \rightarrow \sigma^*_{N2-C3}$) increases from isomer **1** to isomer **2**. The LP(e)$_{S7}$ orbitals occupancies correspondingly increase in the following order: isomer **1** < isomer **2**, while the occupancies of the σ^*_{N2-C3} bonds increase in a parallel manner in the opposite order. Analysis of the NBO charges demonstrated that the C$_3$–S$_7$ bond is polarized in reaction **1** in the sense of C$_3^{\delta+}$–S$_7^{\delta-}$, while in the reaction (2), the rate determining step revealed that the H$_6$–S$_7$ bond is highly polarized both in isomer **2** (as reactant) and TS structures in the sense of H$_6^{\delta+}$–S$_7^{\delta-}$. Analysis of the computed structures, bond orders and free energy profiles demonstrate that the isomerization reactions (1) and (2) satisfy the Hammond principle: the transition state for the chemical reaction (2) is structurally closer to isomer **2**.

SUPPLEMENTARY MATERIAL

Supplementary data (Fig. S-1 and Tables S-I–S-III) associated with this article are available electronically from http://www.shd.org.rs/JSCS/, or from the corresponding author on request.

ИЗВОД

РАЗУМЕВАЊЕ КИНЕТИКЕ ИЗОМЕРИЗАЦИЈЕ У ГАСНОЈ ФАЗИ ДЕРИВАТА ТРИАЗОЛ-3-ТИОНА. ТЕОРИЈСКИ ПРИСТУП

ZAHRA KAZEMINEJAD[1], ABOLFAZL SHIROUDI[2], KHALIL POURSHAMSIAN[1], FARHAD HATAMJAFARI[1] и AHMAD REZA OLIAEY[1]

[1]Department of Chemistry, Tonekabon Branch, Islamic Azad University, Tonekabon, Iran u [2]East Tehran Branch, Islamic Azad University, Tehran, Iran

Реакција изомеризације 4-амино-5-метил-2,4-дихидро-3*H*-1,2,4-триазол-3-тиона проучавана је теоријски користећи теорију функционала густине са различним функционалима измене-корелације (B3LYP и M06-2*x*), те са CBS-QB3 квантнохемијским приступом као репером. Израчунати енергетски профил је допуњен израчунавањем константи брзина реакција на основу теорије прелазног стања. На основу оптимизованих геометрија изомера применом CBS-QB3 методе, анализа природних орбитала веза показује да се делокализација електрона из невезивне природне орбитале слободног пара (LP(e)$_{S7}$) на суседну σ^*_{N2-C3} антивезивну орбиталу повећава од изомера **1** до изомера **2**. Такође, LP(e)$_{S7} \rightarrow \sigma^*_{N2-C3}$ делокализација може лепо да објасни повећање попуњености LP(e)$_{S7}$ невезивних орбитала у прстену код изомера **1** и **2** (**2** > **1**). Делокализација електрона из LP(e)$_{S7}$ невезивних на σ^*_{N2-C3} антивезивне орбитале повећава стабилност структуре основног стања. Због тога, пораст LP(e)$_{S7} \rightarrow \sigma^*_{N2-C3}$ делокализације може донекле објаснити кинетику реакција изомеризација (1) и (2) ($k_2 > k_1$). NBO резултати такође сугеришу да је кинетика ових процеса контролисана LP→σ^* резонанционим енергијама.

REFERENCES

1. B. Namratha, S. L. Gaonkar, *Int. J. Pharm.* **6**(8) (2014) 73
(https://innovareacademics.in/journals/index.php/ijpps/article/view/2778/10493)

2. S. Nekkanti, R. Tokala, N. Shankaraiah, *Curr. Med. Chem.* **24** (2017) 2887 (https://doi.org/10.2174/0929867324666170523102730)
3. J. K. Sahu, S. Ganguly, A. Kaushik, *Chin. J. Nat. Med.* **11** (2013) 456 (https://doi.org/10.1016/S1875-5364(13)60084-9)
4. K. T. Potts, *Chem. Rev.* **61** (1961) 87 (https://doi.org/10.1021/cr60210a001)
5. N. F. Eweiss, A. A. Bahajaj, E. A. Elsherbini, *J. Heterocycl. Chem.* **23** (1986) 1451 (https://doi.org/10.1002/jhet.5570230540)
6. J. M. Kane, M. W. Dudley, S. M. Sorensen, F. P. Miller, *J. Med. Chem.* **31** (1988) 1253 (https://doi.org/10.1021/jm00401a031)
7. S. M. Sorensen, J. M. Zwolshen, J. M. Kane, *Neuropharmacology* **29** (1990) 555 (https://doi.org/10.1016/0028-3908(90)90067-2)
8. Z. Y. Zhang, H. Yan, *Acta Chim. Sin.* **45** (1987) 403 (http://manu19.magtech.com.cn/Jwk_hxxb/EN/abstract/abstract333017.shtml)
9. M. B. Talawar, S. C. Bennur, S. K. Kankanwadi, P. A. Patil, *Indian J. Pharm. Sci.* **57** (1995) 194 (http://www.ijpsonline.com/abstract/antiinflammatory-activity-of-some-new-3substituted4amino5mercapto4h124triazoles-1906.html)
10. T. V. Ghochikyan, M. A. Samvelyan, A. S. Galstyan, S. V. Grigoryan, *Chem. Biol.* **2** (2016) 8 (http://ysu.am/science/en/1465212714)
11. M. S. Al-Khawas, B. A. A. Hazaa, A. S. Al-Din, *Sci. Pharm.* **47** (1979) 314
12. M. D. Davari, H. Bahrami, Z. Zolmajd Haghighi, M. Zahedi. *J. Mol. Model.* **16** (2010) 841 (https://doi.org/10.1007/s00894-009-0585-z)
13. M. Koparir, C. Orek, P. Koparir, K. Sarac, *Spectrochim. Acta, A* **105** (2013) 522 (https://doi.org/10.1016/j.saa.2012.12.052)
14. Nithinchandra, B. Kalluraya, S. Aamir, A. R. Shabaraya, *Eur. J. Med. Chem.* **54** (2012) 597 (https://doi.org/10.1016/j.ejmech.2012.06.011)
15. K. Sztanke, T. Tuzimski, J. Rzymowska, K. Pasternak, M. Kandefer-Szerszeń, *Eur. J. Med. Chem.* **43** (2008) 404 (https://doi.org/10.1016/j.ejmech.2007.03.033)
16. A. Ameri, G. Khodarahmi, F. Hassanzadeh, H. Forootanfar, G.-H. Hakimelahi, *Arch. Pharm. (Weinheim, Ger.)* **349** (2016) 662 (https://doi.org/10.1002/ardp.201600021)
17. G. A. Sandip, R. M. Suleman, S. P. Vandana, *Chem. Asian J.* **6** (2011) 2696 (https://doi.org/10.1002/asia.201100432)
18. P. Ratchanok, P. Veda, M. Prasit, C. Nantasenamat, S. Prachayasittikul, S. Ruchirawat, *Bioorg. Med. Chem.* **23** (2015) 3472 (https://doi.org/10.1016/j.bmc.2015.04.036)
19. R. Kaur, A. R. Dwivedi, B. Kumar, V. Kumar, *Anticancer Agents Med. Chem.* **16** (2016) 465 (https://doi.org/10.2174/1871520615666150819121106)
20. A. N. Syed, M. Gurumurthy, J. C. Swarup, P. Debashisha, *J. Adv. Pharm. Res.* **1** (2010) 26
21. Z. Jin, A. Huo, T. Liu, Y. Hu, J. Liu, J. Fang, *J. Organomet. Chem.* **690** (2005) 1226 (https://doi.org/10.1016/j.jorganchem.2004.11.028)
22. E. Pomarnacka, I. Kozlarska-Kedra,, *Farmaco* **58** (2003) 423 (https://doi.org/10.1016/S0014-827X(03)00071-5)
23. S. Nadeem, A. Waquar, *Eur. J. Med. Chem.* **45** (2010) 1536 (https://doi.org/10.1016/j.ejmech.2009.12.062)
24. J. Chen, X. Y. Sun, K.-Y. Chai, J.-S. Lee, M. S. Song, Z. S. Quan, *Bioorg. Med. Chem.* **15** (2007) 6775 (https://doi.org/10.1016/j.bmc.2007.08.004)
25. A. M. Abdel-Megeed, H. M. Abdel-Rahman, G. S. Alkaramany, M. A. El-Gendy, *Eur. J. Med. Chem.* **44** (2009) 117 (https://doi.org/10.1016/j.ejmech.2008.03.017)
26. B. Tozkoparan, N. Gokhan, G. Aktay, E. Yesilada, M. Ertan, *Eur. J. Med. Chem.* **35** (2000) **743** (https://doi.org/10.1016/S0223-5234(00)00157-4)

27. K. S. Bhat, B. Poojary, D. J. Prasad, P. Naik, B. S. Holla, *Eur. J. Med. Chem.* **44** (2009) 5066 (https://doi.org/10.1016/j.ejmech.2009.09.010)
28. B. S. Holla, B. Veerendra, M. K. Shivananda, B. Poojary, *Eur. J. Med. Chem.* **38** (2003) 759 (https://doi.org/10.1016/S0223-5234(03)00128-4)
29. S. Saha, D. Dhanasekaran, S. Chandraleka, N. Thajuddin, A. Panneerselvam, *Adv. Biol. Res.* **4** (2010) 224 (ISSN 1992-0067)
30. R. Iqbal, N. H. Rama, U. Yunus, A. Saeed, K. Zamani, *J. Chem. Soc. Pak.* **19** (1997) 145 (https://www.jcsp.org.pk/ArticleUpload/1910-8501-1-RV.pdf)
31. L. Fotouhi, F. Hajilari, M. M. Heravi, *Electroanalysis* **14** (2002) 1728 (https://doi.org/10.1002/elan.200290017)
32. H. Gökce, N. Öztürk, Ü. Ceylan, Y. B. Alpaslan, G. Alpaslan, *Spectrochim. Acta, A* **163** (2016) 170 (https://doi.org/10.1016/j.saa.2016.03.041)
33. R. G. Parr, W. Wang, *Density Functional Theory of Atoms and Molecules,* Oxford University Press, New York, Oxford, 1989 (https://doi.org/10.1002/qua.560470107)
34. C. Lee, W. Yang, R. G. Parr, *Phys. Rev., B: Condens. Matter Mater. Phys.* **37** (1988) 785 (https://doi.org/10.1103/PhysRevB.37.785)
35. A. D. Becke, *J. Chem. Phys.* **98** (1993) 5648 (https://doi.org/10.1063/1.464913)
36. Y. Zhao, D. G. Truhlar, *Acc. Chem. Res.* **41** (2008) 157 (https://doi.org/10.1021/ar700111a)
37. Y. Zhao, D. G. Truhlar, *Theor. Chem. Acc.* **120** (2008) 215 (https://doi.org/10.1007/s00214-007-0310-x)
38. T. H. Dunning, Jr., *J. Chem. Phys.* **90** (1989) 1007 (https://doi.org/10.1063/1.456153)
39. J. A. Montgomery, Jr., M. J. Frisch, J. W. Ochterski, G. A. Petersson, *J. Chem. Phys.* **112** (2000) 6532 (https://doi.org/10.1063/1.481224)
40. K. J. Laidler, M. C. King, *J. Phys. Chem.* **87** (1983) 2657 (https://doi.org/10.1021/j100238a002)
41. A. E. Reed, R. B. Weinstock, F. Weinhold, *J. Chem. Phys.* **83** (1985) 735 (https://doi.org/10.1063/1.449486)
42. J. K. Badenhoop, F. Weinhold, *Int. J. Quantum Chem.* **72** (1999) 269 (https://doi.org/10.1002/(SICI)1097-461X(1999)72:4<269::AID-QUA9>3.0.CO;2-8)
43. *Gaussian 09, Revision C.01*, Gaussian, Inc., Wallingford, CT, 2009
44. R. Jasiński, *Comput. Theor. Chem.* **1046** (2014) 93 (https://doi.org/10.1016/j.comptc.2014.08.002)
45. R. Casasnovas, J. Frau, J. Ortega-Castro, A. Salvà, J. Donoso, F. Muñoz, *Int. J. Quantum Chem.* **110** (2010) 323 (https://doi.org/10.1002/qua.22170)
46. F. Fukui, *J. Phys. Chem.* **74** (1970) 4161 (https://doi.org/10.1021/j100717a029)
47. Z. Safaei, A. Shiroudi, R. Padash, M. Sillanpää, E. Zahedi, *J. Fluorine Chem.* **216** (2018) 71 (https://doi.org/10.1016/j.jfluchem.2018.10.009)
48. S. Canneaux, F. Bohr, E. Henon, *J. Comput. Chem.* **35** (2013) 82 (https://doi.org/10.1002/jcc.23470)
49. M. D. Allendorf, T. M. Besmann, R. J. Kee, M. T. Swihart, *Chemical Vapor Deposition: Precursors, Processes and Applications*, 1st ed., The Royal Society of Chemistry, London, 2009 (http://dx.doi.org/10.1039/9781847558794)
50. K. A. Holbrook, M. J. Pilling, S. H. Robertson, *Unimolecular Reactions,* 2nd ed., Wiley, Chichester, 1996 (ISBN 978-0-471-92268-1)
51. E. Wigner, *J. Chem. Phys.* **5** (1937) 720 (https://doi.org/10.1063/1.1750107)
52. E. P. Wigner, *Z. Phys. Chem., Abt. B* **19** (1932) 203 (https://doi.org/10.1515/zpch-1932-0120)

53. *NIST Computational Chemistry Comparison and Benchmark Database, NIST Standard References Database Number 101, section XIII.B.4a: Precomputed vibrational scaling factors*, R. D. Johnson III, Ed. (http://cccbdb.nist.gov/vibscalejust.asp))
54. G. S. Hammond, *J. Am. Chem. Soc.* **77** (1953) 334 (https://doi.org/10.1021/ja01607a027)
55. N. Agmon, R. D. Levine, *Chem. Phys. Lett.* **52** (1977) 197 (https://doi.org/10.1016/0009-2614(77)80523-X)
56. G. Lendvay, *J. Phys. Chem.* **93** (1989) 4422 (https://doi.org/10.1021/j100348a011)
57. A. E. Reed, L. A. Curtiss, F. Weinhold, *Chem. Rev.* **88** (1988) 899 (https://doi.org/10.1021/cr00088a005)
58. K. B. Wiberg, *Tetrahedron* **24** (1968) 1083 (https://doi.org/10.1016/0040-4020(68)88057-3)
59. E. D. Glendening, A. E. Reed, J. E. Carpenter, F. Weinhold, *NBO version 3.1*, Gaussian Inc., Pittsburgh, PA, 2003
60. A. Moyano, M. A. Periclas, E. Valenti, *J. Org. Chem.* **54** (1989) 573 (https://doi.org/10.1021/jo00264a014)
61. F. Rosas, R. M. Dominguez, M. Tosta, J. R. Mora, E. Marquez, T. Cordova, G. Chuchani, *J. Phys. Org. Chem.* **23** (2010) 743 (https://doi.org/10.1002/poc.1646)
62. J. E. Carpenter, F. Weinhold, *J. Mol. Struct.: THEOCHEM* **169** (1988) 41 (https://doi.org/10.1016/0166-1280(88)80248-3).